Electron Spin Resonance Study of Phospholipid Membranes Employing a Comprehensive Line-Shape Model†

A. Lange,‡ D. Marsh,§ K.-H. Wassmer,‡ P. Meier,‡ and G. Kothe*,‡

Institut für Physikalische Chemie der Universität Stuttgart, D-7000 Stuttgart 80, FRG, and Abteilung Spektroskopie, Max-Planck-Institut für Biophysikalische Chemie, D-3400 Göttingen, FRG

Received October 23, 1984; Revised Manuscript Received February 22, 1985

ABSTRACT: The electron spin resonance spectra of the 1-myristoyl-2-[6-(4,4-dimethyloxazolidine-*N*-oxyl)myristoyl]-*sn*-glycero-3-phosphocholine spin-label in highly oriented, fully hydrated bilayers of 1,2-dimyristoyl-*sn*-glycero-3-phosphocholine have been studied as a function of temperature and magnetic field orientation. The oriented spectra show clear indications of slow motional components (rotational correlation times > 3 ns) even in the fluid phase ($T > 23$ °C), indicating that motional narrowing theory is not applicable to the spectral analysis. The spectra have been simulated by a comprehensive line-shape model that incorporates trans–gauche isomerization in addition to restricted anisotropic motion of the lipid long molecular axis and that is valid in all motional regimes. In the gel ($L_{\beta'}$) phase the spin-label chains are found to be tilted at 28° with respect to the normal of the orienting plane. In the intermediate ($P_{\beta'}$) phase there is a continuous distribution of tilt angles between 0° and 25°. In the fluid (L_α) phase there is no net tilt of the lipid chains. The chains rotate at an intermediate rate about their long axis in the fluid phase ($\tau_{R,\parallel}$ = 1.4–6.6 ns for T = 50–25 °C), but the reorientation of the chain axis is much slower ($\tau_{R,\perp}$ = 13–61 ns for T = 50–25 °C), whereas trans–gauche isomerization (at the C-6 position) is rapid ($\tau_J \leq 0.2$ ns). Below the chain melting transition both chain reorientation and chain rotation are at the ESR rigid limit ($\tau_R \geq$ 100 ns), and trans–gauche isomerization is in the slow-motion regime (τ_J = 3.7–9.5 ns for T = 22–2 °C). The chain order parameter increases continuously with decreasing temperature in the fluid phase (S_{ZZ} = 0.47–0.61 for T = 50–25 °C), increases abruptly on going below the chain melting transition, and then increases continuously in the intermediate phase (S_{ZZ} = 0.79–0.85 for T = 22–14 °C) to an approximately constant value in the gel phase ($S_{ZZ} \simeq 0.86$ for T = 10–2 °C). The trans rotational isomer population (corresponding to the C-6 position) remains approximately constant in the fluid phase ($n_t \simeq 0.52$ for T = 50–25 °C) and decreases abruptly at the chain melting transition to a constant value in the intermediate and gel phases ($n_t \simeq 0.44$ for T = 22–2 °C). The results have been compared with those obtained from ^{2}H nuclear magnetic resonance spectroscopy of dimyristoylphosphatidylcholine deuterium labeled at the same position of the *sn*-2 chain. Most of the parameters governing the chain order and dynamics are in good accord, except that the gauche population is considerably higher for the spin-labeled chain and its isomerization rate is much faster in the low-temperature phases. The implications for the interpretation of spin-label measurements in membranes are discussed with particular reference to the well-known discrepancy in the "order gradients" along the chains, obtained by the two methods.

Electron spin resonance (ESR)[1] spectroscopy of spin-labeled lipid molecules is widely used for probing the dynamic structure of lipid bilayers and biological membranes [for reviews, see, e.g., Marsh (1981, 1982) and Marsh & Watts (1982)]. The utility of the method arises because the mobility of spin-label molecules in fluid lipid membranes is found to lie close to the optimum range of motional sensitivity of nitroxide ESR spectroscopy. In principle, the information that can be obtained from the spin-label spectra is the amplitude and rate of motion of the spin-label group and the polarity of the environment in which it is situated. Most spectral analyses so far have used motional-narrowing theory, whereby the spectra are in the fast-motional regime, and the amplitude of motion and an index of the environmental polarity can be derived directly from the measured line splittings. Values for the rate of motion come from the spectral line widths and for anisotropic motion can be determined only by line-shape analysis. Whereas motional-narrowing theory has very successfully been applied to line-shape analysis in soap bilayers (Schindler & Seelig, 1973), the molecular motion in phospholipid bilayers and biological membranes is less rapid, and there are indications that the spectra might no longer be in the fast-motional regime (Cannon et al., 1975; Freed, 1976; Schreier et al., 1978). Consequently, there has to date been no comprehensive line-shape analysis of phospholipid spin-labels in membranes.

A related problem in the analysis of membrane ESR spectra is the extent to which the spin-label motion directly reflects that of the parent, unlabeled host phospholipids. Although there is agreement between spin-label ESR and ^{2}H nuclear magnetic resonance (NMR) on the existence of an "order gradient" along the chains of the lipid molecules in bilayer membranes, the quantitative values of the order parameters

† Financial support by Deutsche Forschungsgemeinschaft and Fonds der Chemischen Industrie is gratefully acknowledged.

‡ Institut für Physikalische Chemie der Universität Stuttgart.

§ Abteilung Spektroskopie, Max-Planck-Institut für Biophysikalische Chemie.

[1] Abbreviations: ESR, electron spin resonance; NMR, nuclear magnetic resonance; DMPC, 1,2-dimyristoyl-*sn*-glycero-3-phosphocholine; DPPC, 1,2-dipalmitoyl-*sn*-glycero-3-phosphocholine; 6-DMPCSL, 1-myristoyl-2-[6-(4,4-dimethyloxazolidine-*N*-oxyl)myristoyl]-*sn*-glycero-3-phosphocholine; CSL, 4′,4′-dimethylspiro[5α-cholestane-3,2′-oxazolidin]-3′-yloxy.

0006-2960/85/0424-4383$01.50/0

for the corresponding labeled chain segments differ between the two methods (Seelig & Seelig, 1974; Taylor & Smith, 1980). Various explanations have been offered for this discrepancy, including the different time scales of the two magnetic resonance methods and associated possible slow-motion effects in the ESR spectra (Gaffney & McConnell, 1974; Mason & Polnaszek, 1978). Clearly the motion of the spin-label group will differ from that of an unlabeled CH_2 group for purely steric reasons (Taylor & Smith, 1983), and it is an important part of the spin-label spectral analysis to assess the magnitude and origin of this distorting effect. From the above discussion it is clear that this can only be done by an accurate line-shape analysis and detailed comparison with the results of ^2H NMR analyzed according to exactly the same motional model.

In the present work we have studied the ESR spectra of a spin-labeled derivative of dimyristoylphosphatidylcholine, with the nitroxide group on the C-6 atom of the *sn*-2 chain, doped in highly oriented bilayers of dimyristoylphosphatidylcholine at maximum hydration. The angular dependence of the spectra gives clear indications of motional contributions in the slow-motional regime. The spectra have been simulated as a function of temperature and magnetic field orientation by a comprehensive line-shape model, which includes the effects of both long axis motion and chain trans–gauche isomerization and which is valid in all motional regimes of spin-label ESR spectroscopy. The results are compared with a corresponding analysis of the ^2H NMR of dimyristoylphosphatidylcholine bilayers labeled at the same methylene segment, by an identical line-shape model.

THEORY

Analysis of the ESR spectra of the spin-labeled phospholipid was achieved by using the comprehensive line-shape model, outlined in the appendix. Here we summarize important features of this treatment and introduce the simulation parameters. The basis of our model is the *stochastic Liouville equation* (Kubo, 1969; Norris & Weissman, 1969; Freed et al., 1971; Kothe, 1977), which we solve by using a finite grid point method. Particular emphasis is given to the slow-motional regime, where the conventional Redfield theory (Redfield, 1965) no longer applies. The line shapes are calculated from a spin Hamiltonian, which considers Zeeman and hyperfine interactions of nitroxide radicals, including *pseudosecular* contributions (Freed, 1976; Wassmer et al., 1985). No adiabatic approximation is applied.

The phospholipid chain motion is simulated by a dynamic model that allows for both *intermolecular* and *intramolecular motions*. The intermolecular motion is the motion of the chain as a whole. It is assumed that the chain axis Z (see Figure 1) undergoes continuous, anisotropic diffusion within an orienting potential. The intramolecular motion consists of trans–gauche isomerization (see Figure 1), which is represented by a jump process. The dynamics of the system are thus characterized by three correlation times. These are $\tau_{R,\parallel}$ and $\tau_{R,\perp}$ for rotation around the chain axis and rotation of the chain axis, respectively, and τ_J the correlation time for trans–gauche isomerization.

Molecular order of the phospholipid chains is described in terms of internal and external coordinates. The internal part accounts for different *conformations* and the external part for different *orientations*. Symmetry considerations suggest that the two gauche conformations per CH_2 group are equally populated (see Figure 1). Thus, conformational order of a chain segment can be characterized by a single parameter, the trans population n_t (gauche population: $2n_g = 1 - n_t$).

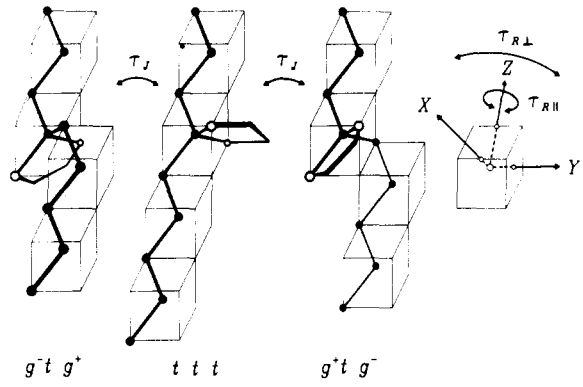

FIGURE 1: Conformations of the spin-labeled phospholipid chain (C3–C11) in its all-trans state (*ttt*) and with a single kink (g^+tg^- or g^-tg^+) at the point of attachment (C6) of the spin-label ring. The axes **X**, **Y**, **Z** indicate the molecular coordinate system that diagonalizes the order and diffusion tensor for the chain. Significant motional modes are represented by arrows. They refer to chain rotation ($\tau_{R,\parallel}$), chain fluctuation ($\tau_{R,\perp}$) and trans–gauche isomerization (τ_J), respectively.

The orientational order of the chains is treated in the meanfield approximation, using an orienting potential such as is common in molecular theories of liquid crystals (Cotter, 1977). The orientational distribution function, given in the appendix, depends on only three parameters, A, δ_{min}, and δ_{max}. The coefficient A characterizes the orientation of the chain axes Z with respect to a local director $\mathbf{z}'$ (net ordering axis), while the parameters δ_{min} and δ_{max} specify the orientation of the director axes in the sample system, defined by the glass plate normal $\mathbf{z}''$ (see Figure 2). It should be noted, that the conventional order parameter, S_{ZZ}, is related to the coefficient A by a mean value integral (Saupe, 1964):

$$S_{ZZ} = (1/2)N_1 \int_0^\pi (3\cos^2\beta - 1)\exp(A\cos^2\beta)\sin\beta\,d\beta \quad (1)$$

$$1/N_1 = \int_0^\pi \exp(A\cos^2\beta)\sin\beta\,d\beta$$

The *microorder* of the phospholipid chains is thus specified by the chain order parameter S_{ZZ} plus the segmental trans population n_t, while the *macroorder* is specified by the values of δ_{min} and δ_{max}, characterizing the director distribution ($\delta_{min} < \delta < \delta_{max}$). In unoriented samples, the director axes $\mathbf{z}'$ are randomly distributed between $\delta_{min} = 0°$ and $\delta_{max} = 180°$. In macroscopically ordered samples, however, $\mathbf{z}'$ may be partially aligned, assuming a fixed tilt angle ($\delta_{min} = \delta_{max} = \delta$) relative to the glass plate normal $\mathbf{z}''$ (see Figure 2).

MATERIALS AND METHODS

Materials. Myristic acid labeled on the C-6 atom [2-(4-carboxybutyl)-2-octyl-4,4-dimethyl-3-oxazolidinyloxyl) was prepared from 6-ketomyristic acid, which was synthesized from 1-bromooctane and adipic acid chloride monomethyl ester (Hubbell & McConnell, 1971). Spin-labeled dimyristoylphosphatidylcholine, 6-DMPCSL, was synthesized by the catalyzed acylation of 1-myristoyl-2-lyso-*sn*-glycerol-3-phosphocholine with the anhydride of the 6-myristic acid spin-label (Mason et al., 1981). Further details of spin-label preparation may be found in Marsh & Watts (1982). Figure 1 shows the structure of the flexible nitroxide radical, together with a molecular coordinate system, which diagonalizes the order and rotational diffusion tensor. 1,2-Dimyristoyl-*sn*-glycero-3-phosphatidylcholine (DMPC) was purchased from Fluka, Buchs, Switzerland, and the purity was controlled by

Table I: Constant Parameters Used in the Calculation of the ESR Spectra of the Phospholipid Spin-Label 6-DMPCSL

hyperfine tensor[a]	g tensor[a]	residual line width[b]	magnetic tensor orientations[c]		
			trans	gauche$^+$	gauche$^-$
$A_{X_K X_K}$ = 0.65 mT	$g_{X_K X_K}$ = 2.0088	$(1/T_2^0)_{41}$ = 0.125 mT	$\varphi_1 = 0°$	$\varphi_2 = -36°$	$\varphi_3 = 72°$
$A_{Y_K Y_K}$ = 0.58 mT	$g_{Y_K Y_K}$ = 2.0061	$(1/T_2^0)_{52}$ = 0.125 mT	$\vartheta_1 = 0°$	$\vartheta_2 = 60°$	$\vartheta = -60°$
$A_{Z_K Z_K}$ = 3.35 mT	$g_{Z_K Z_K}$ = 2.0027	$(1/T_2^0)_{63}$ = 0.125 mT	$\psi_1 = 0°$	$\psi_2 = -72°$	$\psi_3 = 36°$

[a] Diagonal in X_K, Y_K, Z_K. [b] $(1/T_2^0)_{ij}$ decreases with increasing temperature to the limiting value of $(1/T_2^0)_{ij}$ = 0.09 mT and is independent of orientation. [c] Euler angles relating magnetic and diffusion tensor system (see Figures 1 and 2).

thin-layer chromatography. A solvent mixture containing 75% dichloromethane and 25% methanol (v/v) was used to dissolve both the lipid and the spin-label. The solvents were distilled from KOH pellets under nitrogen atmosphere. Dichloromethane was then water saturated. All solutions were prepared immediately before use. The radical concentration was 0.2 mM, while the lipid concentration was 0.2 M.

Sample Preparation. Typically, 30 μL of the above solution, corresponding to 6 nmol of spin-label and 6 μmol or 4 mg of lipid, was uniformly distributed on the bottom of an open quartz flat cell by means of a glass micropipet. The organic solvents were removed by first warming the sample cell on a water bath (60 °C, 1 min) and then placing it under vacuum (0.1 Torr, 25 °C, 15 min). The cell was then immersed into a water-saturated atmosphere (60 °C, 1 min) and finally closed with a tightly fitting cover. The amount of water that commonly condensed onto the sample was 10 mg. The above procedure yielded macroscopically oriented multilayers of high reproducibility (Meier et al., 1982). The quality of the sample was checked before and after each set of ESR experiments by recording ESR spectra under the same conditions.

ESR Measurements. The ESR measurements were performed on a Bruker ER 200D-SRC spectrometer equipped with an X-band microwave bridge (ν = 9.4 MHz), using 100-kHz field modulation. Orientation of the flat sample cell in the laboratory frame was achieved with a home-built goniometer. ESR spectra were measured as a function of temperature and angle ρ between glass plate normal and magnetic field direction (see Figure 2). The temperature control was found to be stable to ±0.25 °C. On recording, the spectra were simultaneously digitized and transferred to a HP 1000 computer for further processing.

Spectral Analysis. A Fortran program was employed to analyze the experimental spectra. The program NOROTJUMP calculates ESR line shapes of flexible nitroxide radicals undergoing fast, intermediate, and slow inter- and intramolecular reorientation in an anisotropic medium. On the basis of the Lanczos algorithm (Moro & Freed, 1981) NOROTJUMP was found to yield accurate line shapes with at least 10-fold reductions in computing time and computer storage requirements compared to the Rutishauser algorithm (Gordon & Messenger, 1972). Typical running time for one spectrum of the nitroxide radical on a HP 1000 computer (F series, 620K memory) is 40 min ($N_A N_B N_K$ = 270). Table I summarizes the constant parameters used in the calculations. The magnetic parameters were obtained from a detailed analysis of fast-motional and rigid-limit spectra. Note that the residual line width $1/T_2^0$ accounts for unresolved proton hyperfine interactions, omitted in the spin Hamiltonian. The orientation of the order and diffusion tensor axes is suggested by the geometry of the spin-labeled lipid (see Figure 1). We assume that the order tensor is axially symmetric along Z. This assumption, tested by spectral simulations, reflects the overall shape of the molecule, which is also expected to exhibit axially symmetric rotational diffusion about the Z axis. The magnetic tensor, defined by the NO group of the oxazolidine ring, may assume

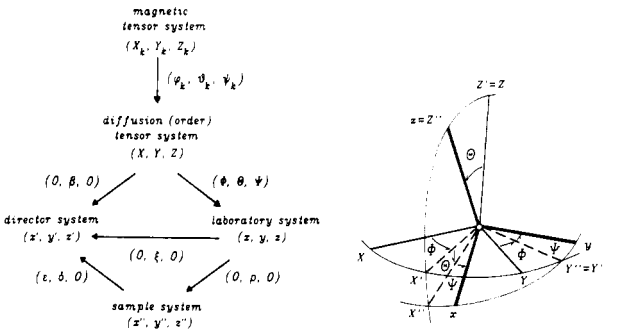

FIGURE 2: Notation for coordinate systems and Euler transformations used in the ESR line-shape model. The various coordinate systems are magnetic tensor system $\mathbf{X_K}$, $\mathbf{Y_K}$, $\mathbf{Z_K}$ ($\mathbf{Z_K}$ = direction of nitrogen $2p_z$ orbital, $\mathbf{X_K}$ = N–O bond direction), diffusion (order) tensor system $\mathbf{X}$, $\mathbf{Y}$, $\mathbf{Z}$ ($\mathbf{Z}$ = phospholipid chain axis), laboratory system $\mathbf{x}$, $\mathbf{y}$, $\mathbf{z}$ ($\mathbf{z}$ = magnetic field direction), director system $\mathbf{x'}$, $\mathbf{y'}$, $\mathbf{z'}$ ($\mathbf{z'}$ = net ordering axis of chains), and sample system $\mathbf{x''}$, $\mathbf{y''}$, $\mathbf{z''}$ ($\mathbf{z''}$ = glass plate normal). The coordinate systems are related by Euler transformations, consisting of three successive rotations. The Euler transformation shown rotates the diffusion tensor system $\mathbf{X}$, $\mathbf{Y}$, $\mathbf{Z}$ into the laboratory system $\mathbf{x}$, $\mathbf{y}$, $\mathbf{z}$. The definition of the Euler angles θ, Φ, and ψ corresponds to that of Van et al. (1974).

three different orientations, relative to the diffusion tensor. The Euler angles φ_K, ϑ_K, and ψ_K characterizing these orientations (see Figure 1) are also listed in Table I.

The remaining adjustable parameters, δ_{min}, δ_{max}, S_{ZZ}, n_t, $\tau_{R,\perp}$, $\tau_{R,\parallel}$, and τ_J are determined by spectral simulations. In general, however, they need not all be evaluated. In macroscopically unoriented samples the director axes are randomly distributed, and thus, δ_{min} and δ_{max} are known. Although this simplifies the analysis, an unambiguous fit of the remaining simulation parameters is generally not possible.

In contrast, spectral analysis of macroscopically aligned samples is unequivocal but more involved. Generally, the simulation parameters affect the line shape in different ways. However, reliable determination of these parameters requires independent variation. Fortunately, in many cases, the director distribution is separately obtained from the angular dependence of the spectral splitting. The remaining parameters S_{ZZ}, n_t, $\tau_{R,\perp}$, $\tau_{R,\parallel}$ and τ_J are then evaluated by computer simulation of a set of seven angular-dependent spectra at any given temperature. An iterative fit of experimental and simulated line shapes generally yields reliable values for all variable parameters.

In some cases, one can extract one motion, which dominates the line shape. This is particularly true if the other motions approach either the fast motion or rigid limit. Having extracted the dominant motion in one such region, its temperature dependence, usually a linear Arrhenius plot, is extrapolated into other regions, where the situation is not so straight forward. The reliability of this procedure has, of course, to be checked by comparing the simulated spectrum with the corresponding experimental one.

The particular sensitivity of the angular-dependent nitroxide ESR line shapes to the variable parameters, characterizing

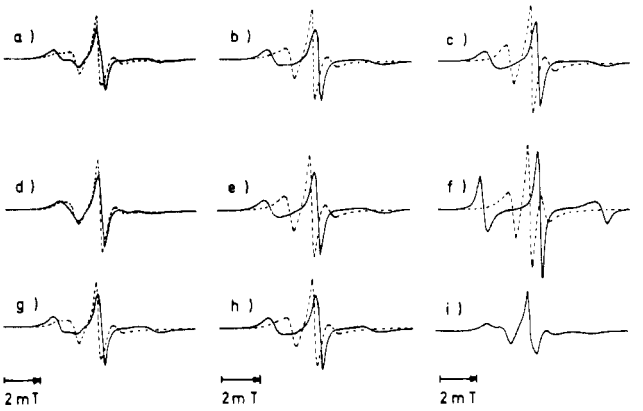

FIGURE 3: Effect of varying the parameters characterizing molecular order on the simulated spectra for oriented samples: (solid line) magnetic field parallel to the bilayer normal ($\rho = 0°$); (broken line) magnetic field oriented perpendicular to bilayer normal ($\rho = 90°$). Constant magnetic parameters are given in Table I. Simulation parameters are $S_{ZZ} = 0.79$, $n_t = 0.5$, $\delta_{min} = \delta_{max} = 0$, $\tau_{R,\perp} = 100$ ns, $\tau_{R,\parallel} = 10$ ns, and $\tau_J = 4.8$ ns, except for the single parameter which is varied. (Upper row) Effect of varying the orientation parameter: (a) $S_{ZZ} = 0.30$, (b) $S_{ZZ} = 0.65$, and (c) $S_{ZZ} = 0.87$. (Middle row) Effect of varying the trans population: (d) $n_t = 0.2$, (e) $n_t = 0.5$, and (f) $n_t = 0.8$. (Lower row) Effect of varying the director distribution: (g) $\delta_{min} = \delta_{max} = 35°$, (h) $\delta_{min} = 0°$ and $\delta_{max} = 35°$, and (i) $\delta_{min} = 0°$ and $\delta_{max} = 180°$.

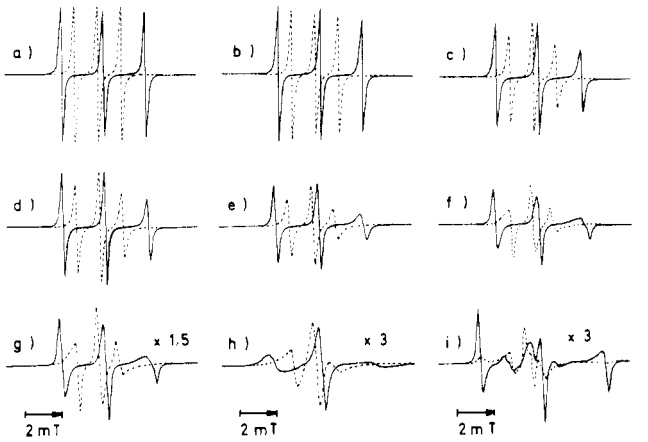

FIGURE 4: Effect of varying the dynamic parameters on the simulated spectra for oriented samples: (solid line) magnetic field oriented parallel to the bilayer normal ($\rho = 0°$); (broken line) magnetic field oriented perpendicular to the bilayer normal ($\rho = 90°$). Constant magnetic parameters are given in Table I. Fixed simulation parameters are $S_{ZZ} = 0.79$, $n_t = 0.5$, and $\delta_{min} = \delta_{max} = 0°$. (Upper row) Effects of varying $\tau_{R,\perp}$ ($\tau_{R,\parallel} = 0.1$ ns, $\tau_J = 0.1$ ns): (a) $\tau_{R,\perp} = 0.1$ ns, (b) $\tau_{R,\perp} = 3.0$ ns, and (c) $\tau_{R,\perp} = 100$ ns. (Middle row) Effect of varying ($\tau_{R,\parallel}$ ($\tau_{R,\perp} = 100$ ns, $\tau_J = 0.1$ ns): (d) $\tau_{R,\parallel} = 0.1$ ns, (e) $\tau_{R,\parallel} = 3.0$ ns, and (f) $\tau_{R,\parallel} = 100$ ns. (Lower row) Effect of varying τ_J ($\tau_{R,\perp} = 100$ ns, $\tau_{R,\parallel} = 100$ ns): (g) $\tau_J = 0.16$ ns, (h) $\tau_J = 4.8$ ns, and (i) $\tau_J = 160$ ns.

molecular order and dynamics, is demonstrated in Figures 3 and 4, respectively. The first row in Figure 3 refers to an increasing chain order parameter S_{ZZ}; the second row refers to different trans populations whereas the third row corresponds to three distinct director distributions. The variation of the spectra with type and time scale of certain molecular motional modes, which are characteristic for flexible alkyl chain spin-labels, is shown in Figure 4. The first row refers to chain fluctuation, and the second and third row reflect chain rotation and trans–gauche isomerization of the labeled segment, respectively. It is noteworthy to realize that spectral parameters such as line intensities or line splittings do in general not relate to particular dynamic or structural features. Consequently, for systems characterized by slow motions, there

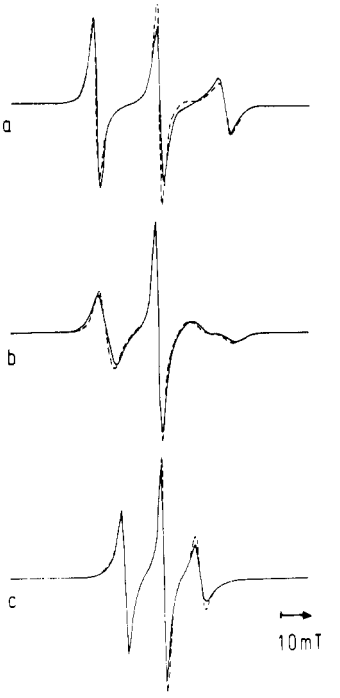

FIGURE 5: Comparison of experimental (—) and simulated (--) ESR spectra of 6-DMPCSL in oriented bilayers of DMPC in the fluid phase, $T = 40$ °C, as a function of magnetic field orientation: (a) $\rho = 0°$; (b) $\rho = 45°$; (c) $\rho = 90°$. Simulation parameters are those given in Tables I and II.

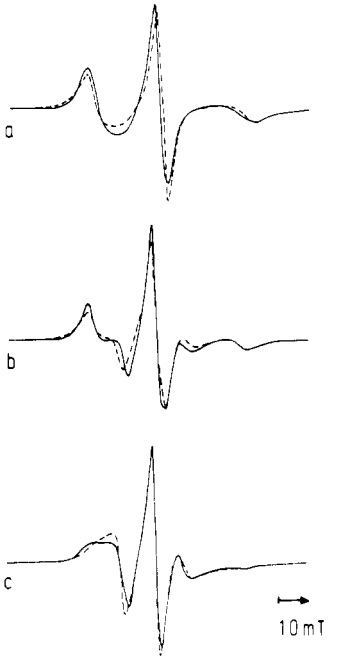

FIGURE 6: Experimental (—) and simulated (--) ESR spectra of 6-DMPCSL in oriented bilayers of DMPC in the intermediate phase, $T = 18$ °C: (a) $\rho = 0°$; (b) $\rho = 45°$; (c) $\rho = 90°$. Simulation parameters are those given in Tables I and II.

is no simple strategy to elucidate the molecular properties from the spectra.

RESULTS

Macroscopically aligned samples of DMPC multibilayers were studied over a wide temperature range (2 °C < T < 50 °C), with the phospholipid spin-label. Typical ESR spectra, varying drastically with temperature and orientation of glass plate normal and magnetic field, are shown in Figures 5–7. They characterize the liquid-crystalline (Figure 5), interme-

Table II: Optimized Parameters Used in the Simulation of the ESR Spectra of the 6-DMPCSL Phospholipid Spin-Label Incorporated into Oriented Bilayers of DMPC

	director distribution[a]			trans population, n_t[c]	correlation times[d]		
T (°C)	δ_{min}	δ_{max}	order parameter S_{ZZ}[b]		$\tau_{R,\perp}$ (ns)	$\tau_{R,\parallel}$ (ns)	τ_J (ns)
50	0	0	0.47	0.51	13	1.4	≤0.2
47	0	0	0.50	0.51	15	1.7	≤0.2
44	0	0	0.51	0.51	19	1.9	≤0.2
40	0	0	0.53	0.51	23	2.3	≤0.2
37	0	0	0.55	0.52	29	2.8	≤0.2
34	0	0	0.55	0.52	35	3.7	≤0.2
30	0	0	0.57	0.53	44	4.4	≤0.2
27	0	0	0.60	0.54	56	5.4	≤0.2
25	0	0	0.61	0.53	61	6.6	≤0.2
22	0	25	0.79	0.45	≥100	≥100	3.7
20	0	25	0.81	0.44	≥100	≥100	3.8
18	0	25	0.83	0.44	≥100	≥100	4.3
16	0	25	0.84	0.44	≥100	≥100	4.5
14	0	25	0.85	0.44	≥100	≥100	4.8
10	28	28	0.86	0.44	≥100	≥100	7.5
8	28	28	0.86	0.45	≥100	≥100	8.0
6	28	28	0.86	0.44	≥100	≥100	8.4
4	28	28	0.86	0.44	≥100	≥100	8.9
2	28	28	0.86	0.45	≥100	≥100	9.5

[a] The uncertainty in fixed tilt angles ($\delta_{min} = \delta_{max}$) is ≤5°. [b] See eq 1. [c] Population of the trans conformation of the sixth chain segment. [d] $\tau_{R,\perp}$ refers to reorientation of the chain axis and $\tau_{R,\parallel}$ to rotation about it. τ_J is the average lifetime of a conformation at the sixth chain segment.

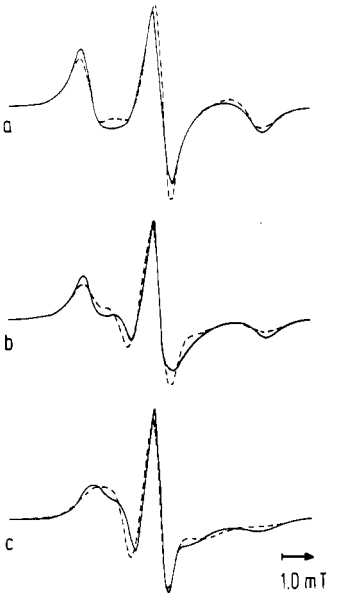

FIGURE 7: Experimental (—) and simulated (--) ESR spectra of 6-DMPCSL in oriented bilayers of DMPC in the gel phase, T = 6 °C: (a) ρ = 0°; (b) ρ = 45°; (c) ρ = 90°. Simulation parameters are those given in Tables I and II, except $(1/T_2^0)_{ij}$ = 0.225 mT.

diate (Figure 6), and gel phase (Figure 7) of the phospholipid membrane. Calculated spectra were fitted to the experimental spectra by applying the procedure outlined above. The dotted lines in Figures 5–7 represent best fit simulations, according to the parameters listed in Table II. The agreement between experimental and calculated spectra is striking. It can be improved slightly by adding spectra, to account for the <5% of unoriented material. This relatively low amount justifies the technique employed for sample preparation (Meier et al., 1982).

Table II summarizes the parameters obtained from the simulations, i.e., the parameters of the director distribution δ_{min} and δ_{max}, the chain order parameter S_{ZZ} (see eq 1), the trans population of the labeled segment n_t, and the correlation times $\tau_{R,\perp}$, $\tau_{R,\parallel}$, and τ_J for inter- and intramolecular motion. The temperature dependence of these parameters is given in Figures 8 and 9, which refer to the molecular dynamics and

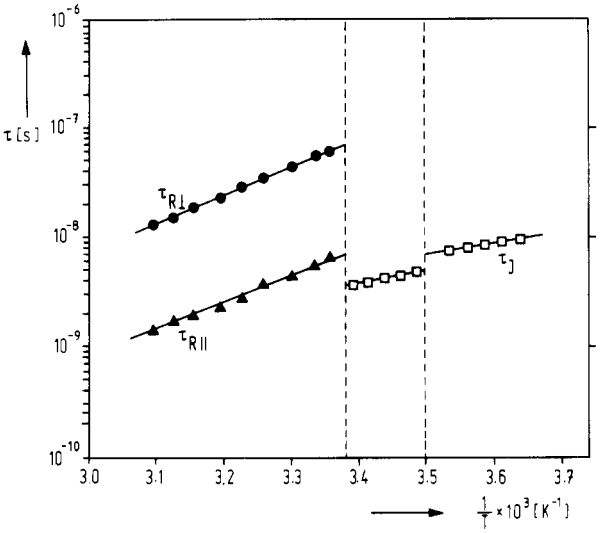

FIGURE 8: Arrhenius plot of the correlation times for chain rotation, $\tau_{R,\parallel}$ (▲), for chain fluctuation, $\tau_{R,\perp}$ (●), and for trans–gauche isomerization, τ_J (□), for 6-DMPCSL in DMPC bilayers.

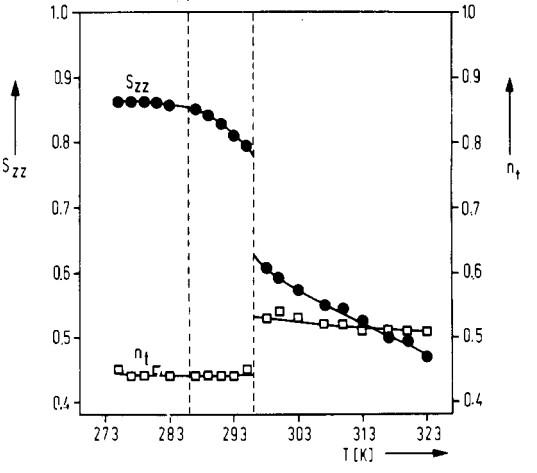

FIGURE 9: Temperature dependence of the chain order parameter, S_{ZZ} (●), and the trans population, n_t (□), for 6-DMPCSL in DMPC bilayers.

Table III: Activation Energies of Chain Motions Characterizing the 6-DMPCSL Spin-Label in the Different Phases of DMPC Bilayers

phase	activation energies for trans–gauche isomerization, E_J (kcal/mol)[a]	chain reorientation	
		$E_{R,\perp}$ (kcal/mol)[b]	$E_{R,\parallel}$ (kcal/mol)[b]
L_α		12.1 ± 0.2	11.7 ± 0.3
$P_{\beta'}$	5.8 ± 0.7		
$L_{\beta'}$	4.7 ± 0.4		

[a] E_J is the activation energy for trans–gauche isomerization at the sixth chain segment. [b] $E_{R,\perp}$ and $E_{R,\parallel}$ refer to chain fluctuation and chain rotation, respectively.

the molecular order, respectively. In the following we describe the results in more detail, treating the three phases separately.

Liquid-Crystalline Phase (L_α Phase). In the L_α phase the director orients parallel to the bilayer normal. The parameter S_{ZZ}, characterizing the local chain order of the phospholipid spin-labels increases with decreasing temperature from $S_{ZZ} = 0.47$ to $S_{ZZ} = 0.61$. In contrast, the trans population $n_t \simeq 0.5$ remains fairly constant. The correlation times $\tau_{R,\perp}$ and $\tau_{R,\parallel}$ for intermolecular chain motion range from 1.5 to 60 ns, implying that a fast-motional line-shape theory (Redfield, 1965) would be inadequate even for the L_α phase. Logarithmic plots of $\tau_{R,\perp}$ and $\tau_{R,\parallel}$ vs. $1/T$ give straight lines. The activation energies evaluated from these plots are $E_{R,\perp} = 12.1$ kcal/mol and $E_{R,\parallel} = 11.7$ kcal/mol, respectively (see Table III). Trans–gauche isomerization can only be characterized by a limiting correlation time $\tau_J \leq 0.2$ ns, thus exhibiting no other effect than fast exchange of the respective conformations. The uncertainty in correlation times for intermolecular motion is <10%.

Intermediate Phase ($P_{\beta'}$ Phase). In the $P_{\beta'}$ phase the director axes are randomly distributed between $\delta_{min} = 0°$ and $\delta_{max} = 25°$. The chain order parameter increases with decreasing temperature from $S_{ZZ} = 0.79$ to $S_{ZZ} = 0.85$, while the trans population remains constant at $n_t \simeq 0.44$. The correlation times for all three motions have significantly dropped at the main transition. $\tau_{R,\perp}$ and $\tau_{R,\parallel}$ are now in the rigid limit and cannot be determined anymore. The only dynamic process affecting the line shape is trans–gauche isomerization with correlation times of $\tau_J \simeq 4$ ns. Indeed, these correlation times and the corresponding trans populations n_t can now precisely be determined. The uncertainty for n_t is ≤0.02, whereas the maximum error for the conformational lifetime is <10%.

Gel Phase ($L_{\beta'}$ Phase). In the $L_{\beta'}$ phase the director distribution changes, showing a fixed tilt angle of $\delta_{min} = \delta_{max} = 28°$. The chain order parameter slightly increases with falling temperature to $S_{ZZ} = 0.86$, while the trans population remains constant at $n_t = 0.45$. The rate of trans–gauche isomerization slows down with a constant activation energy of $E_J = 4.7$ kcal/mol (see Table III). A drastic line broadening, depending on time and on sample history, can be modeled by increasing the line width up to $(1/T_2^0)_{ij} = 0.225$ mT.

In the low-temperature phases two distinct director distributions have been determined. This result demonstrates the power of the method employed, since the two distributions are not particularly different.

Discussion

The experimental results from highly oriented, fully hydrated DMPC bilayers, combined with an analysis using a comprehensive line-shape model, have provided a rather complete description of the chain ordering and dynamics of a flexible phospholipid spin-label in this model membrane system. Previous studies of this kind have been restricted to samples of low water content and to a line-shape model that makes no explicit allowance for trans–gauche isomerization (Meirovitch & Freed, 1980). Other analyses have concentrated on the simpler *rigid* spin-label molecules (Polnaszek et al., 1981; Meier et al., 1982; Dammers et al., 1982) or nematic liquid crystals (Broido & Meirovitch, 1983). In the present work, a line-shape model is used that is based on the *stochastic Liouville equation* (valid for all motional regimes). The spin Hamiltonian includes pseudosecular terms, the adiabatic approximation is not used, and molecular order is considered in terms of internal and external coordinates. The internal part accounts for different conformations and the external part for different orientations. Molecular dynamics is treated by a comprehensive model, which allows for both intermolecular and intramolecular motions (reorientation and isomerization). The ^{2}H NMR spectra of fully hydrated DMPC bilayers, deuterium-labeled at the same position as bears the spin-label group in the present study, have been analyzed by the same line-shape model (Meier et al., 1985), and this provides a means of assessing the differences in ordering and motion of the spin-label group compared with the corresponding unlabeled methylene group of the parent phospholipid molecule. In the following, the results on the molecular dynamics (characterized by the motional correlation times), the macroorder (characterized by the chain director distribution), and the microorder (characterized by the chain order parameter and conformational probability) are discussed in detail separately.

Molecular Dynamics. The chain dynamics are specified in terms of three different correlation times, $\tau_{R,\parallel}$, $\tau_{R,\perp}$, and τ_J. They refer to chain rotation, chain fluctuation, and trans–gauche isomerization, respectively. An Arrhenius plot of the various correlation times is shown in Figure 8. In the fluid (L_α) phase it is possible in principle to determine all three correlation times unambiguously, since there are already slow motional effects *above* the main DMPC phase transition. However, only an upper limit can be put on the value of τ_J because the effects of this fast motion on the spectra are only slight and it is difficult to distinguish these from a simple temperature-dependent intrinsic line width. In the intermediate ($P_{\beta'}$) and gel ($L_{\beta'}$) phases, $\tau_{R,\perp}$ and $\tau_{R,\parallel}$ are in the rigid limit, and therefore, only a lower limit may be put upon their values. The value of τ_J is unambiguously determined in both low-temperature phases.

Compared with ESR, the correlation times for the corresponding deuterium-labeled DMPC (Meier et al., 1985) in the fluid phase can be determined with much less accuracy, since all motions are in the fast regime on the ^{2}H NMR timescale. However, the values obtained for $\tau_{R,\perp}$ and $\tau_{R,\parallel}$ in the fluid phase are similar to those in Table II, and $\tau_J \simeq 0.4$ ns is consistent with the limits given in Table II. In the intermediate phase, $\tau_{R,\perp}$ and $\tau_{R,\parallel}$ are 100–1000 ns, which is consistent with the ESR spectra being in the rigid limit with respect to these correlation times. The values for τ_J in the intermediate and gel phase are, however, 2 orders of magnitude greater than those found for the ESR label.

The activation energies for the two intermolecular motions (Table III) are comparable in the fluid phase and are similar to the values obtained from ^{2}H NMR (Meier et al., 1985). The values of the activation energy for trans–gauche isomerization in the gel and intermediate phases are considerably smaller, in agreement with those obtained by ^{2}H NMR (Meier et al., 1985). The higher activation energies for the intermolecular motions presumably reflect the cooperative nature of these processes. The activation energy for trans–gauche

isomerization ($\simeq$5 kcal/mol) can be compared with 2 times the C–C bond rotational potential barrier height ($\simeq$3 kcal/mol; Flory, 1969) encountered in $g^{\pm}tg^{\mp}$ kink formation (see Figure 1).

The finding of slow motional effects even in the fluid phase has important consequences for the interpretation of lipid spin-label spectra in membranes. Although such effects are not immediately obvious in the ESR spectra from unoriented samples, the spectrum corresponding to 45° magnetic field orientation in Figure 5b is diagnostic in this respect. If this spectrum were in the fast motional regime, it would consist solely of three relatively sharp lines similar to those seen for the 0° and 90° field orientation. For a highly oriented specimen, with the motional axis coinciding with the axis of orientation, such double bumps as seen in the high-field region of Figure 5b are indicative of slow motional contributions, as confirmed by the value of $\tau_{R,\perp} = 23$ ns obtained from simulations. The slow-motion effects will affect the line splittings in unoriented specimens (Freed, 1976) and thus give rise to errors in spin-label order parameters calculated in the usual way from motional narrowing theory.

Macroorder. The macroscopic orientation distribution employed in the simulation program refers to the director specifying the average chain orientation. It is found that there is no net tilt of the phospholipoid chains in the fluid phase ($\delta = 0°$), a spread of tilt angles in the intermediate phase ($0° \leq \delta \leq 25°$), and a fixed tilt angle in the gel phase ($\delta = 28°$). These findings can be compared with the results of other ESR studies and the structural information obtained from X-ray diffraction in the intermediate and gel phases.

A previous ESR study employing a rigid biradical spin probe (Meier et al., 1982) found $\delta = 0°$ in the fluid phase, $0° \leq \delta \leq 19°$ in the intermediate phase, and $\delta = 23°$ in the gel phase, in substantial agreement with the present results. In 1,2-dipalmitoyl-*sn*-glycero-3-phosphocholine (DPPC), a tilt angle of 33° has been estimated by ESR with a phosphatidylcholine spin probe labeled at the C-5 atom, and a somewhat smaller value was obtained with a probe labeled on the C-16 atom (Birrell & Griffith, 1976). This apparent dependence on chain position is understandable in terms of the trans–gauche isomerization in the gel phase found in the present study. A tilt of approximately 25° has also been found for DPPC in the gel phase with the rigid cholestane spin probe CSL (Hemmings, 1975). It should be noted, however, that a rather more approximate method of analysis was employed in the latter two studies and the samples were most likely at less than maximum hydration.

X-ray diffraction studies on DMPC have determined a tilt angle ranging from 35° to 30° in the gel phase, with a net tilt angle of 30° in the intermediate phase (Janiak et al., 1976). It should perhaps be mentioned that these are rather indirect measurements involving assumptions regarding lumped lipid densities and water composition of the phases. The angle of tilt found in the gel phase is comparable to that found in the present study, but the finding of a fixed tilt angle in the intermediate phase is contrary to the present results. However, it is likely that the model employed may not have been able to distinguish between a fixed tilt and a distribution of tilt angles. As discussed previously (Meier et al., 1982), the present results suggest a model for the intermediate phase in which the lipid chains are oriented perpendicular to the local bilayer surface of the rippled phase. Assuming a simple sinusoidal ripple, the amplitude to wavelength ratio

$$a/\lambda = [1/(2\pi)] \tan \delta_{max} \quad (2)$$

results in $a/\lambda = 0.074$, which is in quite good agreement with the value $a/\lambda = 7.5$ Å/118 Å = 0.064 (corresponding to $\delta_{max} = 22°$) found by X-ray diffraction analysis (Janiak et al., 1979).

Microorder. The microorder of the spin-label phospholipid chains is specified by the angular amplitude of reorientation of the chain axis (given by the chain order parameter S_{ZZ}), plus the segmental trans population n_t. As seen from Figure 9, the chain order parameter may be unambiguously determined in all three phases. The values obtained agree closely both with those obtained previously with a rigid biradical spin probe (Meier et al., 1982) and also with the values obtained from a similar analysis of both the 6-position and 14-position deuterium-labeled DMPCs using ^{2}H NMR (Meier et al., 1983, 1985). Similar results have also been obtained with the rigid cholestane spin probe CSL in oriented DMPC bilayers (A. Lange et al., unpublished results).

The trans and gauche isomer populations corresponding to the spin-label 6-position can also be determined in all three phases. However, in this case the values of n_t are considerably different from those derived in a similar fashion from the ^{2}H NMR spectra of the 6-position deuterium-labeled DMPC (Meier et al., 1985). Whereas values of $n_t \simeq 0.51$–0.53 are obtained in the fluid phase by spin-label ESR, the corresponding values derived from ^{2}H NMR are much higher, $n_t \simeq 0.7$–0.75. On going through the main phase transition, the ESR-derived values decrease yielding $n_t \simeq 0.44$ throughout the intermediate and gel phases. In contrast, an increase is deduced from ^{2}H NMR to a nearly constant value of $n_t \simeq 0.9$ throughout the low-temperature phases. These low values of n_t found by ESR almost certainly correspond to a distortion of the local conformational order of the spin-labeled chain needed to accommodate the bulky nitroxide group (cf. Figure 1). The decrease in n_t on going below the main phase transition presumably corresponds to a further distortion induced by the closer molecular packing in the low-temperature phase. These conclusions are in agreement with ^{2}H NMR experiments on a deuterium-labeled phosphatidylcholine spin-label, which have also indicated a local distortion in the orientation of the nitroxide group (Taylor & Smith, 1983).

The result of this is that the net molecular order parameter

$$S_{mol} = S_{ZZ}[(9/8)n_t - 1/8] \quad (3)$$

for a given spin-labeled segment is generally smaller than that exhibited by the unperturbed system. Evidently, the distorting effect of the nitroxide ring, decreasing the local conformational order, is also responsible for the discrepancy in the "order gradients" along the chains, obtained by ESR and ^{2}H NMR for corresponding phospholipids (Seelig & Seelig, 1974; Taylor & Smith, 1980). At the moment it is not known to what extent the distortion varies with chain position. Resolution of this point must await further experiments on other positional isomers.

Conclusions

In summary, the present analysis has shown that the steric effects of the nitroxide group distort the local conformation at the point of label attachment, giving rise to a higher population of gauche rotational isomers. All other parameters governing the chain ordering and motion, including the trans–gauche isomerization rate in the fluid phase, reflect those of the unlabeled chain to within a reasonable degree of accuracy. In particular, the values derived for the chain order parameter faithfully reproduce those for the unlabeled chain. Slow-motion effects are very important even in the fluid phase and must be taken into account in any detailed analysis of lipid spin-labels in membranes. Empirical analysis such as is

commonly applied using motional narrowing theory can only be useful when made by a detailed comparison with the spectral behavior in a series of well-defined model systems (R. D. Pates, A. Watts, and D. Marsh, unpublished results). Of particular interest with regard to the model membrane system under study is the existence of a continuous distribution of director orientations ($0° \leq \delta \leq 25°$) in the ripple phase of DMPC and the finding of slow modes of reorientation of the chain axis ($\tau_{R,\perp} \simeq$ 13–61 ns for T = 50–25 °C) in the fluid lipid membrane phase.

ACKNOWLEDGMENTS

We thank Frau G. Angerstein for her chemical expertise in the preparation of the spin-label and Dr. E. Ohmes for his assistance in the computations. Part of the numerical calculations were carried out on a Univac 1100/60 at the Computer Center of the University of Stuttgart.

APPENDIX

In this appendix we briefly develop an ESR line-shape model for flexible nitroxide spin probes, undergoing *inter- and intramolecular motion* (i.e., both chain reorientation and isomerization) in an anisotropic medium. Generally, the absorption line shape $L(\omega)$ for an ensemble of radicals is given by

$$L(\omega) = \mathrm{Im}[\mathrm{tr}(\rho \cdot \mathbf{S}_+) \exp(-i\omega t)] \tag{A-1}$$

where $\mathbf{S}_+$ is the raising operator, ω is the angular frequency of the microwave field, and ρ is the spin density matrix, assumed to obey the *stochastic Liouville equation* (Kubo, 1969; Norris & Weissman, 1969; Freed et al., 1971; Kothe, 1977):

$$\dot{\rho}_{ABK} = (i/\hbar)[\rho_{ABK} \cdot \mathbf{H}_{ABK}] + (\dot{\rho}_{ABK})_{relax} + (\dot{\rho}_{ABK})_{rot} + (\dot{\rho}_{ABK})_{isom}$$

$$(\dot{\rho}_{ABK})_{rot} = \sum_{A'} (\mathbf{k}_{A'ABBKK} \cdot \rho_{A'BK} - \mathbf{k}_{AA'BBKK} \cdot \rho_{ABK}) + \sum_{B'} (\mathbf{k}_{AAB'BKK} \cdot \rho_{AB'K} - \mathbf{k}_{AABB'KK} \cdot \rho_{ABK})$$

$$(\dot{\rho}_{ABK})_{isom} = \sum_{K'} (\mathbf{k}_{AABBK'K} \cdot \rho_{ABK'} - \mathbf{k}_{AABBKK'} \cdot \rho_{ABK}) \tag{A-2}$$

Here $\mathbf{H}_{ABK}$ is the spin Hamiltonian of the radical, $(\dot{\rho}_{ABK})_{relax}$ is a phenomenological relaxation term, and $(\dot{\rho}_{ABK})_{rot}$ and $(\dot{\rho}_{ABK})_{isom}$ account for the inter- and intramolecular motion of the radicals, respectively. It is assumed that only a finite number of angular positions or sites, denoted by the index ABK, can be occupied during this process. Each site is characterized by a set of Euler angles (θ_A, Φ_B, φ_K, ϑ_K, ψ_K) relating the magnetic system $\mathbf{X}_K$, $\mathbf{Y}_K$, $\mathbf{Z}_K$ through a diffusion tensor system $\mathbf{X}$, $\mathbf{Y}$, $\mathbf{Z}$ to the laboratory system $\mathbf{x}$, $\mathbf{y}$, $\mathbf{z}$, which we choose with the z axis parallel to the magnetic field (see Figure 2).

In the basis of the Zeeman functions $|M_S, M_I\rangle$

$$|1\rangle = |1/2, 1\rangle$$
$$|2\rangle = |1/2, 0\rangle$$
$$|3\rangle = |1/2, -1\rangle$$
$$|4\rangle = |-1/2, 1\rangle$$
$$|5\rangle = |-1/2, 0\rangle$$
$$|6\rangle = |-1/2, -1\rangle \tag{A-3}$$

the matrices $\mathbf{k}_{AA'BBKK}$ in eq A-2 are multiples of the unit matrix, characterizing the rate at which radicals at site ABK move into site A'BK. The values for the transition rates depend upon the model used to describe the motion. For the intermolecular motion (chain reorientation), a diffusive process is assumed (rotation through a sequence of infinitesimally small angular steps). In that case the transition rates must satisfy the equations (Kothe et al., 1979):

$$k_{AA+1BBKK} + k_{AA-1BBKK} = N_A^2/(3\pi^2\tau_{R,\perp})$$
$$k_{AABB+1KK} + k_{AABB-1KK} = N_B^2/(12\pi^2\tau_{R,\parallel})$$
$$k_{AA'BBKK} n_{ABK} = k_{A'ABBKK} n_{A'BK}$$
$$k_{AABB'KK} n_{ABK} = k_{AAB'BKK} n_{AB'K} \tag{A-4}$$
$$\text{A and A'} = 1, 2, 3, \ldots, N_A$$
$$\text{B and B'} = 1, 2, 3, \ldots, N_B$$

where N_A and N_B are the number of orientations in θ and Φ, respectively. Solving eq A-4, one can establish values for all transition rates in terms of two rotational correlation times, $\tau_{R,\perp}$ and $\tau_{R,\parallel}$, and the equilibrium populations, n_{ABK}, of the sites. $\tau_{R,\perp}$ is the correlation time for reorientation of the symmetry axis of the diffusion tensor, while $\tau_{R,\parallel}$ refers to rotation about it (see Figure 1).

For the intramolecular motion a random jump process is assumed (isomerization through jumps between different conformations). Consequently (Sillescu, 1971)

$$k_{AABBK'K} = n_K/\tau_J \tag{A-5}$$
$$\text{K and K'} = 1, 2, \ldots, N_K$$

where N_K, τ_J, and n_K are the total number of conformations, the average residence time in one conformation, and the relative occupation probability, respectively.

The equilibrium population, n_{ABK}, of a particular site can be expressed as

$$n_{ABK} = n_{AB} n_K \tag{A-6}$$

where n_{AB} is related to the normalized orientational distribution function

$$f(\theta,\Phi,\psi) = N_1 \exp[A(\cos\theta\cos\xi - \sin\theta\cos\psi\sin\xi)^2] \tag{A-7}$$

by an integration over the area of that site:

$$n_{AB} = \int_{\theta_A-\Delta\theta/2}^{\theta_A+\Delta\theta/2} \int_{\Phi_B-\Delta\Phi/2}^{\Phi_B+\Delta\Phi/2} \int_0^{2\pi} f(\theta,\Phi,\psi) \sin\theta \, d\theta \, d\Phi \, d\psi \tag{A-8}$$

$$\Delta\theta = \pi/N_A$$
$$\Delta\Phi = 2\pi/N_B$$

In deriving eq A-7 from statistical theories of nematic liquid crystals (Cotter, 1977) we assumed that the order tensor is axially symmetric in $\mathbf{X}$, $\mathbf{Y}$, and $\mathbf{Z}$. The coefficient A in eq A-7 characterizes the orientation of the radicals with respect to a local director $\mathbf{z}'$ (net ordering axis), while the angle ξ specifies the orientation of $\mathbf{z}'$ in the laboratory frame $\mathbf{x}$, $\mathbf{y}$, $\mathbf{z}$ (Figure 2). In unoriented samples, the director axes are randomly distributed. In macroscopically ordered samples, however, $\mathbf{z}'$ can be specified with respect to a sample system $\mathbf{x}''$, $\mathbf{y}''$, and $\mathbf{z}''$, generally defined by the glass plate, used to prepare the sample. If ρ denotes the angle between $\mathbf{z}''$ (glass plate normal) and $\mathbf{z}$ (magnetic field direction), $\cos\xi$ is found to be

$$\cos\xi = \cos\delta\cos\rho - \sin\delta\cos\epsilon\sin\rho \tag{A-9}$$

where ϵ and δ are the polar coordinates of the director in the sample system (Figure 2). Of course, all director axes need not have the same orientation; instead, they may be distributed according to the adopted simple probability function:

$$f(\epsilon,\delta) = N_2 \quad \text{if} \quad \delta_{min} \leq \delta \leq \delta_{max}$$
$$= 0 \quad \text{otherwise} \tag{A-10}$$

where N_2 is a normalization constant.

The spin Hamiltonian for a nitroxide radical may be written as

$$H_{ABK} = \mu_B(g_{zz})_{ABK}B_zS_z + (A_{xz})_{ABK}S_zI_x + (A_{yz})_{ABK}S_zI_y + (A_{zz})_{ABK}S_zI_z + H_{n\text{-}sec} + H_{rf} \quad \text{(A-11)}$$

where

$$H_{rf} = \mu_B g B_1 S_x \exp(i\omega t) \quad \text{(A-12)}$$

and μ_B, $(g_{zz})_{ABK}$, g, $(A_{zz})_{ABK}$, B_z, B_1, S, and I are the Bohr magneton, the zz component of the g tensor, the isotropic g factor, the zz component of the hyperfine tensor, the static magnetic field, the microwave field, the electron spin operator, and the ^{14}N nuclear spin operator, respectively. Since nonsecular terms $H_{n\text{-}sec}$ are only important at very rapid tumbling rates, which can be treated by the usual perturbation theory (Redfield, 1965; Luckhurst & Zannoni, 1977), we will ignore their effect.

The tensor elements in eq A-11 are orientation dependent; consequently, they fluctuation in time as the radical reorients. We can evalute this orientation dependence by a 2-fold transformation from the magnetic system $\mathbf{X}_K$, $\mathbf{Y}_K$, $\mathbf{Z}_K$, which diagonalizes the g and hyperfine tensor (Hubbell & McConnell, 1971). In the first step we transform to the diffusion tensor system $\mathbf{X}$, $\mathbf{Y}$, $\mathbf{Z}$ by using the Euler rotation matrix $\mathbf{T}(\varphi_K,\vartheta_K,\psi_K)$ (Van et al., 1974):

$$(\mathbf{g}_{X,Y,Z})_K = \mathbf{T}(\varphi_K,\vartheta_K,\psi_K)\cdot(\mathbf{g}_{X_K,Y_K,Z_K})\cdot\mathbf{T}'(\varphi_K,\vartheta_K,\psi_K)$$

$$(\mathbf{A}_{X,Y,Z})_K = \mathbf{T}(\varphi_K,\vartheta_K,\psi_K)\cdot(\mathbf{A}_{X_K,Y_K,Z_K})\cdot\mathbf{T}'(\varphi_K,\vartheta_K,\psi_K) \quad \text{(A-13)}$$

In the second step we rotate by the Euler angles $(\Phi_B,\theta_A,0)$ into the laboratory system $\mathbf{x}$, $\mathbf{y}$, $\mathbf{z}$, and obtain

$$(\mathbf{g}_{x,y,z})_{ABK} = \mathbf{T}(\Phi_B,\theta_A,0)\cdot(\mathbf{g}_{X,Y,Z})_K\cdot\mathbf{T}'(\Phi_B,\theta_A,0)$$

$$(\mathbf{A}_{x,y,z})_{ABK} = \mathbf{T}(\Phi_B,\theta_A,0)\cdot(\mathbf{A}_{X,Y,Z})_K\cdot\mathbf{T}'(\Phi_B,\theta_A,0) \quad \text{(A-14)}$$

Evaluating the density matrix equation of motion (eq A-2) in the basis of the Zeeman functions (eq A-3) gives $36N_AN_BN_K$ coupled differential equations:

$$\dot{\rho}_{ijABK} = (i/\hbar)\sum_l(\rho_{ilABK}H_{ijABK} - H_{ilABK}\rho_{ijABK}) - \rho_{ijABK}[1/(T_2^0)_{ijABK} + k_{AA+1BBKK} + k_{AA-1BBKK} + k_{AABB+1KK} + k_{AABB-1KK} - k_{AABBKK'}] + \rho_{ijA-1BK}k_{A-1ABBKK} + \rho_{ijA+1BK}k_{A+1ABBKK} + \rho_{ijAB-1K}k_{AAB-1BKK} + \rho_{ijAB+1K}k_{AAB+1BKK} + \rho_{ijABK'}k_{AABBK'K} + (i/\hbar)\mu_B g B_1 \exp(i\omega t)\{\sum_l[\rho_{ilABK}(S_x)_{lj} - (S_x)_{il}\rho_{ljABK}]\} \quad \text{(A-15)}$$

$$i, j, \text{ and } l = 1, 2, \ldots, 6$$

where $(1/T_2^0)_{ijABK}$ is a residual line width, and the non-zero matrix elements are given by

$$H_{11ABK} = (1/2)\mu_B(g_{zz})_{ABK}B_z + (1/2)(A_{zz})_{ABK}$$

$$H_{22ABK} = (1/2)\mu_B(g_{zz})_{ABK}B_z$$

$$H_{33ABK} = (1/2)\mu_B(g_{zz})_{ABK}B_z - (1/2)(A_{zz})_{ABK}$$

$$H_{44ABK} = -H_{11ABK},\ H_{55ABK} = -H_{22ABK},\ H_{66ABK} = -H_{33ABK}$$

$$H_{12ABK} = \left(\sqrt{2}/4\right)[(A_{xz})_{ABK} - i(A_{yz})_{ABK}]$$

$$H_{21ABK} = \left(\sqrt{2}/4\right)[(A_{xz})_{ABK} + i(A_{yz})_{ABK}]$$

$$H_{23ABK} = -H_{45ABK} = -H_{56ABK} = H_{12ABK}$$

$$H_{32ABK} = -H_{54ABK} = -H_{65ABK} = H_{21ABK}$$

$$(S_x)_{14} = (S_x)_{25} = (S_x)_{36} = (S_x)_{41} = (S_x)_{52} = (S_x)_{63} = 1/2 \quad \text{(A-16)}$$

For a weak microwave field we can take a steady-state solution of eq A-15 and replace the density matrix elements of the last term by their thermal equilibrium values:

$$\rho^0_{ijABK} = \delta_{ij}n_{ABK}\exp[-H_{ijABK}/(kT)]/\{\mathrm{Tr}(\exp[-H_{ijABK}/(kT)])\} \quad \text{(A-17)}$$

To proceed, we introduce

$$\rho_{ijABK} = \sigma_{ijABK}\exp(i\omega t) \quad \text{(A-18)}$$

and separate the exponential. In the steady state (slow passage)

$$\dot{\sigma}_{ijABK} = 0 \quad \text{(A-19)}$$

and four sets of $9N_AN_BN_K$ coupled linear algebraic equations result. At high fields the solution of only one set is required, which is readily accomplished by employing the Lanczos algorithm (Moro & Freed, 1981). Summing up all contributions according to eq A-1 finally gives the total line shape:

$$L(\omega) = \mathrm{Im}(\sqrt{2}\sigma_{41} + \sqrt{2}\sigma_{52} + \sqrt{2}\sigma_{63}) \quad \text{(A-20)}$$

Registry No. DMPC, 18194-24-6.

REFERENCES

Birrell, G. B., & Griffith, O. H. (1976) *Arch. Biochem. Biophys. 172*, 455–462.

Broido, M. S., & Meirovitch, E. (1983) *J. Phys. Chem. 87*, 1635–1643.

Cannon, B., Polnaszek, C. F., Butler, K. W., Eriksson, E. G., & Smith, I. C. P. (1975) *Arch. Biochem. Biophys. 167*, 505–518.

Cotter, M. A. (1977) *J. Chem. Phys. 66*, 1098–1106.

Dammers, A. J., Levine, Y. K., & Tjon, J. A. (1982) *Chem. Phys. Lett. 88*, 198–201.

Flory, P. J. (1969) *Statistical Mechanics of Chain Molecules*, Wiley-Interscience, New York.

Freed, J. H. (1976) in *Spin Labelling. Theory and Applications* (Berliner, L. J., Ed.) Vol. I, pp 53–132, Academic Press, New York.

Freed, J. H., Bruno, G. V., & Polnaszek, C. F. (1971) *J. Phys. Chem. 75*, 3385–3399.

Gaffney, B. J., & McConnell, H. M. (1974) *J. Magn. Reson. 16*, 1–28.

Gordon, R. G., & Messenger, J. (1972) in *Electron Spin Relaxation in Liquids* (Muus, L. T., & Atkins, P. W., Eds.) pp 341–381, Plenum Press, New York.

Hemminga, M. A. (1975) *Chem. Phys. Lipids 14*, 151–173.

Hubbell, W. L., & McConnell, H. M. (1971) *J. Am. Chem. Soc. 93*, 314–326.

Janiak, M. J., Small, D. M., & Shipley, G. G. (1976) *Biochemistry 15*, 4575–4580.

Janiak, M. J., Small, D. M., & Shipley, G. G. (1979) *J. Biol. Chem. 264*, 6068–6078.

Kothe, G. (1977) *Mol. Phys. 33*, 147–158.

Kothe, G., Wassmer, K.-H., Naujok, A., Ohmes, E., Rieser, J., & Wallenfels, K. (1979) *J. Magn. Reson. 36*, 425–434.

Kubo, R. (1969) in *Stochastic Processes in Chemical Physics, Advances in Chemical Physics* (Shuler, K. E., Ed.) pp 101–127, Wiley, New York.

Luckhurst, G. R., & Zannoni, C. (1977) *Proc. R. Soc. London, Ser. A 353*, 87–102.

Marsh, D. (1981) in *Membrane Spectroscopy* (Grell, E., Ed.) pp 51–142, Springer-Verlag, West Berlin.

Marsh, D. (1982) in *Techniques in Lipid and Membrane Biochemistry* (Hesketh, T. R., & Metcalfe, J. C., Eds.) Vol. B4/II, pp B426/1–B426/44, Elsevier, Ireland.
Marsh, D., & Watts, A. (1982) in *Lipid-Protein Interactions* (Jost, P. C., & Griffith, O. H., Eds.) Vol. 2, pp 53–126, Wiley-Interscience, New York.
Mason, R. P., & Polnaszek, C. F. (1978) *Biochemistry 17*, 1758–1760.
Mason, J. T., Broccoli, A. V., & Huang, C. (1981) *Anal. Biochem. 113*, 96–101.
Meier, P., Blume, A., Ohmes, E., Neugebauer, F. A., & Kothe, G. (1982) *Biochemistry 21*, 526–534.
Meier, P., Ohmes, E., Kothe, G., Blume, A., Weidner, J., & Eibl, H.-J. (1983) *J. Phys. Chem. 87*, 4904–4912.
Meier, P., Ohmes, E., & Kothe, G. (1985) *J. Chem. Phys.* (submitted for publication).
Meirovitch, E., & Freed, J. H. (1980) *J. Phys. Chem. 84*, 3281–3295.
Moro, G., & Freed, J. H. (1981) *J. Chem. Phys. 74*, 3757–3773.
Norris, J. R., & Weissman, S. I. (1969) *J. Phys. Chem. 73*, 3119–3124.
Polnaszek, C. F., Marsh, D., & Smith, I. C. P. (1981) *J. Magn. Reson. 43*, 54–64.
Redfield, A. G. (1965) *Adv. Magn. Reson. 1*, 1–32.
Saupe, A. (1964) *Z. Naturforsch., A 19A*, 161–171.
Schindler, H., & Seelig, J. (1973) *J. Chem. Phys. 59*, 1841–1850.
Schreier, S., Polnaszek, C. F., & Smith, I. C. P. (1978) *Biochim. Biophys. Acta 515*, 375–436.
Seelig, A., & Seelig, J. (1974) *Biochemistry 13*, 4839–4845.
Sillescu, H. (1971) *J. Chem. Phys. 54*, 2110–2119.
Taylor, M. G., & Smith, I. C. P. (1980) *Biochim. Biophys. Acta 599*, 140–149.
Taylor, M. G., & Smith, I. C. P. (1983) *Biochim. Biophys. Acta 733*, 256–263.
Van, S. P., Birrell, G. B., & Griffith, O. H. (1974) *J. Magn. Reson. 15*, 444–459.
Wassmer, K.-H., Ohmes, E., Portugall, M., Ringsdorf, H., & Kothe, G. (1985) *J. Am. Chem. Soc. 107*, 1511–1519.

Internal Motions of Band 3 of Human Erythrocytes†

Bruce Campbell,‡ Enrico Bucci,* and Robert F. Steiner
Department of Biological Chemistry, University of Maryland at Baltimore, Baltimore, Maryland 21201, and Department of Chemistry, University of Maryland Baltimore County, Catonsville, Maryland 21228
Received September 26, 1984; Revised Manuscript Received January 23, 1985

ABSTRACT: Band 3 was labeled with *N*-[[(iodoacetyl)amino]ethyl]-5-naphthylamine-1-sulfonate either exofacially in the intact washed erythrocytes or endofacially by treating inside-out vesicles. Exo labeling resulted in the labeling of several other proteins, besides band 3, which could not be removed from the membrane. Therefore, the exo-labeled band 3 was extracted and purified by chromatography on DEAE-cellulose in Triton X-100. The endo labeling also resulted in the labeling of several other proteins. In this case, washing with NaOH removed all labeled material except band 3 from the vesicles. The lifetime of bound *N*-[(acetylamino)ethyl]-5-naphthylamine-1-sulfonate was heterogeneous, suggesting the positioning of the label in different environments either because different sites were labeled or because of positional freedom of the label at the same point of attachment. The main fraction of emission intensity had a lifetime near 20 ns, as expected for a hydrophobic environment. The rest showed a lifetime of about 3 ns in the exo-labeled band 3 and 9 ns in the endo-labeled band 3. Both lifetimes appeared to be independent of temperature between 5 and 25 °C, suggesting shielding of the probe from the solvent. Quenching phenomena must be responsible for both the 3- and 9-ns lifetimes, not due to residual heme, as proven by the persistence of such quenching in the Triton X-100 extracted protein. The correlation times indicated the presence of a short component, between 2 and 4 ns in the different systems, probably due to the presence of a flexible portion in the structure of the protein. In the endo-labeled system, the anisotropy at long times failed to reach a zero value, consistent with the hypothesis that the rotational motions of the membrane-embedded protein are constrained around a single axis, perpendicular to the plane of the lipid bilayer. Addition of 300 mM NaCl to the samples increased the value of the limiting anisotropy in the endo-labeled system and in the exo-labeled protein decreased the extent of depolarization produced by the motion corresponding to the short correlation time of the system. This suggests an increased rigidity of the system upon addition of NaCl.

Band 3 is the major membrane-spanning glycoprotein of the human erythrocyte with a molecular weight of 95 000 and is the site of the electroneutral anion-exchange reaction. In addition, band 3 acts as a binding site for a number of intracellular proteins such as aldolase (Murthy et al., 1981), glyceraldehyde-3-phosphate dehydrogenase (Yu & Steck, 1975b), phosphofructokinase (Higashi & Richards, 1979), hemoglobin (Shaklay et al., 1977), and band 2.1 of the erythrocyte cytoskeleton (Hargreaves et al., 1980).

The structure and disposition of band 3 in the membrane have been well documented (Drickamer, 1976, 1978; Steck et al., 1976; Appell & Low, 1981; Tsai et al., 1982; Ramjeesingh et al., 1983) although the complete primary structure

† This work was supported in part by National Institutes of Health Grants HL-13164 and AM-30322. Computer time and facilities were supported in part by the computer network of the University of Maryland.
* Address correspondence to this author at the Department of Biological Chemistry, University of Maryland at Baltimore, 660 W. Redwood St., Baltimore, MD 21201.
‡ Present address: Department of Biochemistry, Harvard University School of Medicine, 25 Shattuck St., Boston, MA 02115.

0006-2960/85/0424-4392$01.50/0